HHS Public Access

Author manuscript

Dev Biol. Author manuscript; available in PMC 2018 July 16.

Published in final edited form as:

Dev Biol. 2017 June 01; 426(1): 56–68. doi:10.1016/j.ydbio.2017.04.006.

Cell origin, volume and arrangement are drivers of articular cartilage formation, morphogenesis and response to injury in mouse limbs

Rebekah S. Decker[a,1], **Hyo-Bin Um**[a], **Nathaniel A. Dyment**[b,2], **Naiga Cottingham**[a], **Yu Usami**[a,3], **Motomi Enomoto-Iwamoto**[a], **Mark S. Kronenberg**[b], **Peter Maye**[b], **David W. Rowe**[b], **Eiki Koyama**[a], and **Maurizio Pacifici**[a]

[a]Division of Orthopaedic Surgery, The Children's Hospital of Philadelphia, Philadelphia, PA 19104

[b]Department of Reconstructive Sciences, School of Dental Medicine, University of Connecticut Health Center, Farmington, CT 06030

Abstract

Limb synovial joints are composed of distinct tissues, but it is unclear which progenitors produce those tissues and how articular cartilage acquires its functional postnatal organization characterized by chondrocyte columns, zone-specific cell volumes and anisotropic matrix. Using novel *Gdf5*^{CreERT2} (*Gdf5-CE*), *Prg4-CE* and *Dkk3-CE* mice mated to R26-*Confetti* or single-color reporters, we found that knee joint progenitors produced small non-migratory progenies and distinct local tissues over prenatal and postnatal time. Stereological imaging and quantification indicated that the columns present in juvenile-adult tibial articular cartilage consisted of non-daughter, partially overlapping lineage cells, likely reflecting cell rearrangement and stacking. Zone-specific increases in cell volume were major drivers of tissue thickening, while cell proliferation or death played minor roles. Second harmonic generation with 2-photon microscopy showed that the collagen matrix went from being isotropic and scattered at young stages to being anisotropic and aligned along the cell stacks in adults. Progenitor tracing at prenatal or juvenile stages showed that joint injury provoked a massive and rapid increase in synovial *Prg4*+ and CD44+/P75+ cells some of which filling the injury site, while neighboring chondrocytes appeared unresponsive. Our data indicate that local cell populations produce distinct joint tissues and that

Correspondence to: Rebekah S. Decker; Maurizio Pacifici.

[1]Current address: Genomics Institute of The Novartis Research Foundation, San Diego, CA 92121.
[2]Current address: Department of Orthopaedic Surgery, University of Pennsylvania, Philadelphia, PA 19104.
[3]Current address: Department of Oral Pathology, Osaka University, Osaka 565-0871, Japan

Competing interests

The authors declare no competing or financial interests.

Author contributions

R.S.D. and M.P. designed the study. R.S.D, H-B.U. and N.C. carried out most experiments and analyses. E.K. carried out morphogenetic and gene expression assessments. N.A.D., Y.U. and M.E.I. participated in data gathering. M.K., P.M. and D.W. R. created transgenic lines in collaboration with M.P. and contributed to data analyses. R.S.D. and M.P. co-wrote the paper with suggestions from co-authors.

articular cartilage growth and zonal organization are mainly brought about by cell volume expansion and topographical cell rearrangement. Synovial *Prg4+* lineage progenitors are exquisitely responsive to acute injury and may represent pioneers in joint tissue repair.

Keywords

Synovial joint formation; limb development; articular cartilage growth and morphogenesis; progenitor cell fate; genetic cell tracing; Prg4; Gdf5; Dkk3; tissue repair; mouse

Introduction

Synovial joints are complex, diverse and anatomically fitted structures that are of obvious and crucial importance for body function and quality of life (Archer et al., 1999; Mow and Sugalski, 2001). Articular cartilage in particular has received a great deal of attention owing to its essential role in joint movement, but also its disease susceptibility and poor repair capacity (Caldwell and Wang, 2015; Huey et al., 2012; Johnstone et al., 2013). In adults, the tissue displays a zonal organization and an abundant and unique extracellular matrix (Hunziker et al., 2007). The superficial zone consists of flat tightly-bound cells that sustain frictionless joint motion by producing hyaluronan and Prg4/lubricin (Jay et al., 2001). The intermediate zone is made of oval chondrocytes oriented randomly and separated by appreciable matrix. The deep zone is thick and made of large, round chondrocytes aligned in vertical columns perpendicular to the articular surface and separated by abundant inter-columnar resilient matrix. These structural and organizational features are needed for articular cartilage function (Hunziker et al., 2007; Mow et al., 1992), but it remains unclear how the tissue acquires and maintains them normally (Decker et al., 2014b). It is also not fully clear from where joint progenitors originate and how they bring about tissue formation, growth and morphogenesis.

In newborn mouse knees, the entire prospective articular cartilage is a thin and dense tissue consisting of 6 to 8 layers of small, randomly-oriented *Proteoglycan 4* (*Prg4*) and *Tenascin-C* (*TnC*) expressing cells with scant matrix (Iwamoto et al., 2007; Rhee et al., 2005). It is only over postnatal life that the tissue grows in thickness and acquires its distinct zonal organization and cell columnar arrangement (Gannon et al., 2015; Julkunen et al., 2009), while the total number of cell layers remains about the same. How this transition occurs is a question that has vexed researchers for years. The discovery of cells with a progenitor character in the superficial zone of adult articular cartilage was received with a great deal of interest, particularly as a possible tool to enhance tissue repair (Dowthwaite et al., 2003; Williams et al., 2010). It also led to the suggestion that similar progenitors would be present in neonatal articular tissue and form articular cartilage by a mechanism of apposition, in which the progenitors would proliferate and produce vertical columns of daughter cells encompassing the full thickness of mature cartilage (Dowthwaite et al., 2003; Hunziker et al., 2007). This model was further examined in recent cell lineage studies using knock-in (heterozygous null) *Prg4*^{GFPCreERt2} mice (Kozhemyakina et al., 2015). Following tamoxifen injection at E17.5, *Prg4*^{GFPCreERt2}/*R26-LacZ*-positive (*Prg4+*) cells were found to form a single surface layer in incipient articular tissue at P0, become more numerous over time and

then produce full-thickness columns of articular chondrocytes by 6–8 weeks of age. Though plausible, this model leaves several questions unanswered, including why only the most superficial cells would have this function, why cells would adopt different volumes in different zones over time, and how the cells would become oriented along specific axes. Given the importance of these questions, we reexamined them using new transgenic *Prg4*^{CreERT2} (*Prg4*-CE), *Dkk3*^{CreERT2} (*Dkk3*-CE) and *Gdf5*^{CreERT2} (*Gdf5*-CE) mice, in addition to *Gdf5Cre* mice we originally used to identify the mesenchymal interzone as the initial birth site of embryonic limb joint progenitors (Koyama et al., 2008). Our data do not wholly sustain a model of appositional growth. Rather, we find that articular cartilage growth and thickening mainly rely on formation of non-daughter cell stacks and cell rearrangement, with limited contribution by cell proliferation and a major role played by zone-specific cell volume increases. We also find that embryonically- or adult-generated CD44+/P75+ progenitors cells with *Prg4* lineage character in synovium appear to be exquisitely sensitive to acute cartilage injury.

Materials and methods

Mouse strains

Commercial strains from Jackson Laboratory were: *Gt(ROSA)26Sor*$^{tm9(CAG-tdTomato)}$; *Gt(ROSA)26Sor*$^{tm6(CAG-ZsGreen1)}$; *R26R-Confetti (Gt(ROSA)26Sor*$^{tm1(CAG-Brainbow2.1)Cle}$; *Prg4*^{GFPCreERt2}; *Gt(ROSA)26Sor*$^{tm4(ACTB-tdTomato,-EGFP)Luo}$; and *Gt(ROSA)26Sor*^{tm1Sor}. *Gdf5*Cre and *Prg4*mCherry mice were described previously (Decker et al., 2014a; Koyama et al., 2008). Animal experiments were approved by the IACUC at our respective Institutions. The various sets of data described in the present study were gathered and verified in a minimum of six independent experiments.

Generation of BAC transgenic Dkk3-CE, Gdf5-CE and Prg4-CE inducible Cre mice

DNA Constructs—Murine BAC clones RP23-55N5, RP23-158D24, and RP24-400O24 containing the genes for *Prg4, Dkk3*, and, *Gdf5* respectively were obtained from the Children's Hospital Oakland Research Institute (CHORI). pLD53.SC2-EGFP and PSV1.RecA vectors were kindly provided by Shiaoching Gong (Gong et al., 2010). pCAG-CreERT2 was obtained from Addgene (gift from Dr. Connie Cepko, plasmid #14797).

Assembly of pLD53.SC2-CreERT2—Using pCAG-CreERT2 as a template, CreERT2 was PCR amplified using Phusion DNA polymerase (Finnzyme) and cloned into the pLD53.SC2 after double digestion with Not1 and Sac1 restriction endonucleases. During this cloning procedure, the multiple cloning site was modified to contain Not1, Swa1, BsiW1, and Mlu1 upstream of a Kozak sequence and translational start site using the oligonucleotide sequences, Forward 5'-TCACGCGGCCGCATTTAAATCGTACGACGCGTTGAGCCGCCACCATGTCCAATTTAC TGACC-3' and Reverse 5'-CACTGAGCTCTATCAAGC TGTGGCAGGGAAACCCTCTGCCT-3' for PCR amplification.

Cloning of Homology Arms into pLD53.SC2-CreERT2—Homology arms for *Prg4, Dkk3*, and *Gdf5* were synthesized by high-fidelity PCR, gel purified and restriction digested.

For *Prg4*, a 625bp region of homology one nucleotide upstream of the translational start site was amplified from RP23-55N5 using oligonucleotide sequences Forward 5'-CTCTGGGCCCGCTATATAAGACTTCCAGCACACTGGAGA-3 and Reverse 5'-CTCTACGCGTGTTCTCGGATGCAACGCCCTTGCTTGAGA-3' containing PspOMI and Mlu1 restriction endonuclease sites. For *Dkk3*, a 564bp region of homology immediately upstream of the translational start site was amplified from RP23-158D24 using oligonucleotide sequences Forward 5'-CTCTGCGGCCGCATCGCGATGGGAGGAGGATG-3' and Reverse 5'-CTCTACGCGTGTTTGTTCCGCGCTGGCCGCCGCCTGTG-3' containing Not1 and Mlu1 restriction endonuclease sites. For *Gdf5*, a 215bp region of homology one nucleotide upstream of the translational start site was amplified from RP24-400O24 using oligonucleotide sequences Forward 5'-CTCTGGCGCGCCGTCTGGACACGGGAGCACTTCCACT-3' and Reverse 5'-CTCTACGCGTCTCTGGCCAGCCGCTGAATGACACCAC-3' containing Asc1 and Mlu1 restriction endonuclease sites. Using standard cloning methods, homology arms for *Prg4* and *Dkk3* were cloned into pLD53.SC2-CreERT2 after its digestion with Not1 and Mlu1, while the homology arm for *GDF5* was cloned into the Mlu1 and Asc1 sites of pLD53.SC2-CreERT2.

Bacterial recombination to introduce CreERT2 into desired BAC clones— Recombinase A was introduced into host bacteria containing RP23-55N5, RP23-158D24, and RP24-400O24 by transformation with pSV1.RecA vector (100 ng) and selected for on chloramphenicol (12.5 μg/ml) + tetracycline (10 μg/ml) LB agar plates. Bacteria containing RecA were then transformed by electroporation with 1ug (1–2 μl) of the pLD53.SC2-CreERT2 containing the appropriate homology arm for the specific BAC clone. SOC medium (1 ml) was added and transformed bacteria were incubated with shaking at 200 rpm for one hour at 30°C. Recombinants were first selected for by adding 5 ml of LB medium containing chloramphenicol (12.5 μg/ml), ampicillin (50 μg/ml), and tetracycline (10 μg/ml) to bacteria and grown overnight at 30°C with shaking at 200 rpm. Further selection for recombinant clones was carried out by plating 100 μl of overnight culture onto chloramphenicol (12.5 μg/ml) + ampicillin (50 μg/ml) LB agar plates and incubated overnight at 42°C. Chloramphenicol and ampicillin resistant colonies were screened by colony PCR using primers flanking the 5' end of the homology arm: recomPrg4 Forward 5'-GGACTAATTGGTTCATCCCAGTCCA-3', recomDkk3 Forward 5'-GGTGGTCATCGTCGTGGAGATAG-3' and recomGdf5 Forward 5'-TTTCAGCTGCTGACTGGAGACG-3' and all combined with the primer recomCreERT2 Reverse 5'-CTGGCCCAAATGTTGCTGGATAGTTTTTACT-3'. Colony PCR identified candidate recombinants, which were further verified by diagnostic restriction enzyme digestion and field inversion gel electrophoresis.

BAC Purification and Pronuclear Injection—BAC constructs were purified from 100-ml cultures using a Maxi Kit (Qiagen) with minor modifications. During alkaline lysis, 2M potassium acetate was used in place of a 3M solution. Additionally, after elution with QF buffer, two phenol/chloroform extractions followed by one chloroform extraction were carried out to further clean up the BAC DNA. BAC DNA (12ug) was then linearized with

Not1-HF restriction endonuclease (NEB) for 4–5 hours and loaded onto a CL-4B Sepharose (Sigma) column pre-equilibrated with injection buffer (10 mM Tris, pH7.5, 0.1 mM EDTA, 100 mM NaCl). Forty 250 μl fractions were collected from the column and DNA concentrations were measured with a Nanodrop Spectrophotometer (Thermo-Scientific). Thirty microliters of alternating fractions were also run on a field inversion gel to assess the DNA quality. Separated modified BAC fragments were chosen for pronuclear injection, which was carried out within a day at the UCONN Health Center Gene Targeting and Transgenic Facility. PCR genotyping for Cre recombinase was used to identify transgenic animals using the following oligonucleotide sequences: forward 5'-GCACTTAGCCTGGGGGTAACTA-3' and reverse 5'-GTCATCCTTAGCGCCGTAAATC-3'.

Tamoxifen administration

For timed pregnancy experiments, female *Cre* mice were mated to homozygous male reporter mice overnight and separated in the morning. Noon on the day of separation was considered E0.5. Pregnant *Gdf5*-CE and *Prg4*-CE/R26-Confetti mice received intraperitoneal injections of hydroxytamoxifen (Sigma H7904) suspended at 10 mg/ml in corn oil (MP Biomedical 901414) at a dose of 0.075 mg/gr. All other mouse strains received tamoxifen (Sigma T5648) suspended at 10 or 20 mg/ml in corn oil at a dose of 0.075 mg/gr, with the exception of pregnant $Prg4^{GFPCreERt2}$ mice which were administered a single 4 mg injection at E17.5 as previously described (Kozhemyakina et al., 2015). Expression patterns of R26-tdTomato or R26-zsGreen reflected mRNA expression patterns at the time of injection in *Dkk3*-CE (Supplementary Fig. 2), *Gdf5*-CE (Fig. 4A, Supplementary Fig. 3) and *Prg4*-CE (Supplementary Fig. 1A–B). There was no evidence of ROSA reporter expression in absence of tamoxifen administration in any of the mouse lines studied (data not shown). Notably, efficiency of *R26*-reporter expression within joint tissues was variable. Using the same *Gdf5*Cre line crossed with various *R26*-reporter lines, we found robust cell labeling in *R26*-tdTomato, *R26*-zsGreen and *R26*-LacZ lines (Supplementary Fig. 6A–C, F), and more limited labeling when crossed with *R26*-mTmG *or R26*-Confetti lines (Supplementary Fig. 6D–E,G). Reporter allele was invariably heterozygous in all mice used.

Tissue processing

Tissue samples were fixed overnight at RT in 4% paraformaldehyde before dehydration and paraffin embedding (Decker et al., 2014a; Koyama et al., 2008). Postnatal samples were decalcified in 10% ETDA for 7–14 days before embedding. For frozen sections, samples were fixed overnight at 4°C in 2% paraformaldehyde before progressive cryopreservation in 10, then 20% sucrose until no longer buoyant. Embryonic and P0 samples were embedded in OCT compound (Sakura Tissue-Tek4513), frozen and sectioned at 12 μm. Postnatal samples were decalcified as above, or embedded directly in OCT and sectioned on cryofilm (type IIC, Section-Lab) (Kawamoto and Kawamoto, 2014). Sections were mounted on glass slides and cover-slipped with Vectashield mounting medium containing DAPI (Vector Labs H1400).

Imaging and 3D reconstruction

Bright and dark-field images were taken with a SPOT insight camera (Diagnostic Instruments, Inc.) operated with SPOT 5.1 software. Dark-field images were pseudo colored using Photoshop (V CS5.1, Adobe) and overlaid onto bright field images of the same sample. A Leica TCS LSI confocal microscope with accompanying software was used for imaging of fluorescently labeled frozen tissue sections. For imaging of whole mount samples, knees were disarticulated to expose the surface of the tibia. Samples were partially embedded in 1% agarose, leaving the tibial surface exposed, and immersed in PBS. An upright laser scanning confocal microscope with 2-photon capability (SP5, Leica) was used to obtain 1 μm section images throughout the depth of articular cartilage. 3-D reconstructions of stacked images were created using Volocity software (V6.3, PerkinElmer). Stacked composites were also used to determine total chondrocyte cell volume *in situ* with the use of Imaris software (V. 8.1.2; Bitplane, Zurich, Switzerland)

EdU and TUNEL assays

EdU (Life Technology A1004) was administered intraperitoneally once or 10 times over 10 consecutive days at 50 or 100 mg/kg body weight as indicated. Knee samples were processed for serial sectioning as described above, and the Click-iT EdU AlexaFluor imaging kit reaction (Invitrogen C10337) was used according to manufacturer's protocol. An *in situ* cell detection kit (Roche 11684817910) was used to detect cell apoptosis.

X-gal staining

Immediately after collection, tissue samples used for X-gal staining were placed in tissue fixative (BG5C; Millipore) on ice for 20 min. Staining was performed on frozen sections or intact limbs using X-gal substrate (BG3G; Millipore) according to standard procedures. After staining of intact limbs, limbs were processed for OCT embedding and cryo-sectioning.

Immunohistochemical staining

Immunohistochemistry was completed on 12 μm frozen sections prepared as above. Antigen retrieval was performed by placing slides in 1% SDS for 5 min. Slides were treated for endogenous peroxidase activity by incubating in 3% H_2O_2 for 10 min. Blocking was performed in 1% goat serum. The following primary antibodies were used: Ki67 (Abcam ab16667, 1:50), CD44 (Santa Cruz sc-18849, 1:100) and P75 (Abcam ab71822, 1:100). After overnight incubation at 4°C, slides were washed in TBS and incubated with species-appropriate biotinylated secondary antibody (1:200) at room temperature for 1 hr. Finally slides were incubated for 1 hr with Streptavidin Alexa 647 (Molecular Probes S21374, 1:200) and mounted with DAPI containing medium.

In situ hybridization

In situ hybridization was carried out as described (Koyama et al., 1999) overnight in 4% paraformaldehyde before dehydration and paraffin embedding. Sections were treated for 15 min with a freshly prepared solution of 0.25% acetic anhydride in triethanolamine buffer and were hybridized with antisense or sense ^{35}S-labeled riboprobes (approximately 1×10^6 DPM/

section) at 50°C for 16 hrs. *cDNA* clones used as templates included: *ColX* (nt. 1302-1816; NM009925); *Gdf5* (1321-1871; NM_008109); *Prg4* (41-2646; AB034730); and *Dkk3* (2500-3000; XM_006508014).

RNA isolation and RT-PCR

Articular cartilage was harvested from the tibia at P0 by blunt dissection under a stereomicroscope. Tissue was disrupted using microcentrifuge grinder pestles (Bel-Art Products, Wayne, NJ). Total RNA was extracted using the RNeasy Micro Kit protocol (Qiagen). RNA samples were reverse transcribed using the Quantiscript Reverse transcription system (Qiagen) according to manufacturer's protocol. The following primer sets were designed to span mouse *Prg4* exons 1–5: 5'-TACTTCCCGTCTGCTTGTCG-3' and 5'ATTATCCAGCCCGCTTCCAG-3'

Cartilage injury model

Focal osteochondral defects were created in trochlear groove of 8–12 week-old mice using mice using custom tools (Fitzgerald et al., 2008). At least 6 animals were evaluated for each experimental group. Mice were anesthetized using 1–2% isoflurane. Knee joint was exposed via a small medial para-patella skin incision, joint capsule was opened, and the patella was luxated to expose the trochlear groove and create the defect. Mice were cared for using required post-operation treatment and procedures and were weight-bearing within 2 hr after surgery.

Results

Stacks of non-daughter cells form during postnatal articular cartilage growth

If most superficial *Prg4+* lineage progenitors drive postnatal articular cartilage growth by columnar apposition of daughter cells as proposed by others, this mechanism should be readily verified using R26-*Confetti* reporter mice in which individual cells are traced by random and persistent acquisition of one of four color reporters (GFP, YFP, RFP and CFP), thereby permitting simultaneous tracking of distinct cell progenies and their developmental roles (Snippert et al., 2010). Thus, we mated R26-*Confetti* mice with our transgenic *Prg4-CE* mice, injected pregnant mothers with tamoxifen at E17.5 and monitored limb joints in their pups over time. We focused on medial tibia articular cartilage that displays the complex and multi-zone organization seen in larger mammals including humans and where the joint is exposed to main loads (Rhee et al., 2005). Rather than being restricted to a single superficial layer at P0 (Kozhemyakina et al., 2015), *Prg4-CE/R26-Confetti+* cells (including *Prg4*-expressing cells and their lineage progeny, collectively defined as *Prg4-CE+*) were scattered throughout the *entire* 6–8 cell layers of incipient medial articular cartilage (Fig. 1A–B), very much in line with the fact that all those cells contain *Prg4* transcripts at both E17.5 and P0 (Koyama et al., 2008; Rhee et al., 2005) (see Fig. S1A). The same was seen after injection at E17.5 and collection at P0 in: *Prg4-CE/R26-tdTomato* (Fig. S1B); *Dkk3-CE/R26-zsGreen* mice, with *Dkk3* being another early joint cell marker (Witte et al., 2009) (Fig. 4O below; Fig. S2); and knock-in $Prg4^{GFPCreERt2}$ used previously (Kozhemyakina et al., 2015) and obtained commercially (Fig. S1D–E). With increasing postnatal time, the *Prg4-CE+* cells produced small and locally-restricted clusters of same-color daughter cells

averaging 3–6 cells each (Fig. 1C–E, arrowheads), indicating that their proliferation was low as was their mobility (see Fig. 3 and S4 below for direct proliferation analyses). While there was some evidence of vertical and horizontal cluster expansion, uniquely colored clusters did not usually form full-thickness columns of same-color daughter cells in mature tissue at 1.5 to 2 months of age (Fig. 1E, arrowheads). This was even more apparent by computer-assisted 3D reconstruction in which individual cell groups could be evaluated in their overall spatial arrangement and conformation (Movie 1). Together, the data raised the novel possibility that chondrocyte columns formed through a mechanism of rearrangement and realignment of neighboring cells and groups.

To verify and extend the data, we mated R26-*Confetti* mice with *Gdf5Cre* mice to genetically trace joint progenitors from an earlier embryonic stage and in greater numbers. At P0, many *Gdf5Cre+* cells expressing different reporters were present throughout the prospective tibial articular layers (Fig. 1F–G). At 2 months, same-color cell clusters were small and oriented perpendicular (Fig. 1H, red arrow) and parallel (Fig. 1I, yellow arrow) to articular surface. As above, the chondrocyte columns present at this age were composed of cells expressing different reporters in a mosaic pattern (Fig. 1H–K). 3D analysis and reconstruction revealed that rather than being fully aligned with each other in vertical columns, the cells formed “stacks” of partially overlapping cells, providing further support for the idea above that rearrangement of neighboring cells subtends growth and thickening of mature cartilage (Movie 2).

Gdf5 is expressed at early embryonic days -though minimally by E18.5 (Fig. S3)- and it is thus possible that sequential *Cre*-mediated recombination could have occurred within single early cells, complicating our analyses and conclusions. As pointed out by the creators of the *Confetti* line (Snippert et al., 2010), sequential recombination is a rare event and we very rarely observed double-labeled cells (Fig. 1J, arrowhead). To verify our data however, we examined conditional *ROSA-CE/R26-Confetti* mice injected with tamoxifen at E17.5. Similar mosaic labeling patterns were seen in both the articular layers at P0 (Fig. 1L) and the chondrocyte stacks at 2 months (Fig. 1M–N). Absence of same reporter daughter cell columns was not due to technical limitations of the R26-*Confetti* line, since stereotypic columns of fully overlapping and same reporter-expressing chondrocytes –each generated by a single progenitor from the reserve zone- were present in tibial growth plates of *ROSA-CE/R26-Confetti* mice injected once with tamoxifen (Fig. 1O, arrowheads). It is important to note that the absence of same reporter daughter cells spanning the entire articular cartilage thickness in adult mouse tibia was also reported in a just published study (Li et al., 2016), at variance with the data reported previously (Kozhemyakina et al., 2015) but in line with our data here.

Cell volume is a major driver of postnatal articular growth

To further clarify mechanisms by which tibial articular cartilage achieves its mature thickness, we quantitatively assessed its cellular organization through postnatal life. As expected, incipient medial articular tissue in P0 tibia was thin and highly cellular (Fig. 2A–B, bracket) and was distinguished by *Prg4* and *TnC* expression (Fig. 2C, E) and lack of *Matrillin-1 (Matn-1)* expression (Fig. 2D) (Hyde et al., 2007). By P14, articular cartilage

had increased in thickness and its boundary with underlying secondary ossification center was delineated by *Matn1* and *Collagen X* (*Col X*) expression (Figure 2I–J). It was between P14 and P28 that the tissue underwent a remarkable increase in thickness (Fig. 2F, K) quantified by image analysis (Fig. 2R, blue line), but proliferation of superficial and deeper cells at either stage as revealed by Ki67 staining was minimal compared to P0 (Fig. 3A–C). By P28 and more so by 2 months, the tissue acquired its mature zonal architecture in which: the superficial *Prg4*-expressing zone was about 10 μm thick and formed 6–8% of total cartilage thickness; the intermediate zone, consisting of frequently paired chondrocytes at an angled orientation to the surface, was about 15 μm thick; and the deep zone -with its typical large round chondrocytes in vertical stacks- was about 90 μm thick (Fig. 2K–P). A characteristic “tidemark” delineated the boundary between deep zone and calcified zone (Fig. 2K, O, arrowhead). Second harmonic generation with 2-photon microscopy showed that cell rearrangement and stack formation over time were accompanied by changes in distribution of collagen fibrils that went from being isotropic and scattered at P14 (Fig. 2G) to being anisotropic and aligned along the stacks by P28-2 months (Fig. 2L, P) (Hughes et al., 2005). Quantitative imaging showed that cellularity was maximal in neonatal cartilage with an average of 3–5 cells per 100 μm^2 and decreased to less than half by P14 and thereafter (Fig. 2R, red line), likely reflecting accumulation of extracellular matrix within the tissue. Reciprocally, the tissue reached its maximal thickness at about P28 (Fig. 2R). The deep zone constituted the bulk of the tissue from P14 on, and the relative heights of superficial and transitional and calcified zones became stabilized by P28 (Fig. 2Q). Studies have suggested that articular cartilage grows by a process of cell resorption and neoformation in some species (Hunziker et al., 2007). However, we detected minimal cell death in articular tissue at P0 or P14, with rare TUNEL-positive cells located primarily at the surface (Fig. 3E, F, arrowheads). TUNEL-positive cells became evident by P28 and more so at 2 months, particularly in the deep zone (Fig. 3G, H, arrowheads). As cell proliferation was low while cell death was higher during the period of substantial growth from P0 to P28 (Fig. 3N), cell death may have roles in adult tissue consolidation and cell density regulation (Fig. 2Q). It should be noted that the very low degree of cell proliferation observed at P28 by Ki67 staining (Fig. 3C, D) is in sharp contrast with a high degree of proliferation reported by Kozhemyakina et al. (2015) after 10 consecutive EdU daily injections. To address this apparent discrepancy, we reassessed proliferation using an identical protocol (10 consecutive daily EdU injections) and same EdU dose (50 mg/kg), but still found that cell proliferation was minimal, amounting to about 3% of cells (Fig. S4). Thus, regardless of whether an endogenous marker (Ki67), an exogenous label (EdU) or cell cluster size (see below) was used as criteria, proliferation of joint cells at P28 was minimal.

Because cell density decreased while cell volume increased over time, the data suggested a reciprocal contribution of these parameters to overall tissue growth. To quantify them, we performed multi-photon imaging of intact tibial cartilage from *ROSA*-CE/R26-*Confetti* mice injected with tamoxifen once at E13.5, P0, P7 or P14, and determined cell number and volume within same reporter (daughter) cell clusters over time. Analysis at 2 months showed that *ROSA-CE+* cells labeled at E13.5 produced the largest clusters, with a maximum of 18 daughter cells (Fig. 3I, M). Cluster size declined markedly thereafter, and averaged about 3–4 cells after P0 induction and about 1–2 cells with increasing age (Fig. 3J–M). To quantify

cell volume, we used 3D reconstruction of *R26-tdTomato* reporter-labeled cells within intact proximal tibial articular tissue and measured their volume using Imaris Software. Average cell volume was lowest at P0, as expected of the compact tissue present at that age (Fig. 3O, Q). While volume of superficial zone cells remained stable (not shown), chondrocyte volume in intermediate and deep zones increased over 3 fold by P14 and P28 and reached a maximum of about 8 fold by 2 months (Fig. 3P, Q). Interestingly, the maximal diameter of deep zone chondrocytes was about 60% of that of collagen X-expressing hypertrophic chondrocytes in secondary ossification center below articular cartilage (Fig. 2J and Fig. S5A–D), and was less than 50% of that of typical metaphyseal growth plate hypertrophic chondrocytes. This indicates that chondrocytes can set their volume at distinct levels depending on location and function (Ginzberg et al., 2015; Youn et al., 2006) and can express distinct phenotypes within each articular zone (Jenner et al., 2014). In sum, while articular cell proliferation had dwindled significantly by P7 and thereafter, cell volumes exhibited a reverse pattern and increased substantially in parallel with tissue thickening from P7 on. The data indicate that while localized proliferation plays a role in early tissue growth, a major mechanism for thickening of articular cartilage over time is provided by cell volume increases and local alignment of non-daughter cells to form stacks perpendicular to the articular surface.

Gdf5-expressing cells contribute to several joint-associated tissues

Gdf5-expressing cells constitute the initial joint mesenchymal interzone in embryonic limbs and produce diverse joint tissues over time (Koyama et al., 2008). Our data above indicate that clonal progenies of cells were rather static and did not migrate much from their site of birth, suggesting that their ability to produce distinct and anatomically diverse tissues may reflect local specification and positional information. To assess this thesis, we developed a novel transgenic G*df5*-CE line and used it to trace and track the cells starting at different stages of joint development. Pregnant *Gdf5*-CE/R26-zsGreen mice were injected with tamoxifen once at E13.5, E15.5 or E17.5, and the resulting *Gdf5-CE+* progenies were monitored in their pups over time. In the structurally simpler and developmentally younger digit joints, cells labeled at E13.5 were limited to the prospective capsule and synovial lining (Fig. 4A), and those patterns had not changed much by P28 (Fig. 4B). Cells labeled at E15.5 or E17.5 were present in both articular layers and capsule by P0 (Fig. 4C, E, yellow arrowhead and red arrow, respectively), and these patterns also did not change significantly with age (Fig. 4D, F) indicating that the *Gdf5*-expressing cells contribute to formation of distinct joint tissues over time.

If distinct tissues arise via spatio-temporally restricted mechanisms, the initial *Gdf5*-expressing interzone cells should diversify over time and express different markers at different locations. Thus, we compared the distribution of constitutive *Gdf5Cre/R26-zsGreen* cell progenies with those in *Dkk3*-CE*/R26-zsGreen* and *Prg4*-CE*/R26-tdTomato* mice induced with tamoxifen once at E17.5 or P28. In line with our previous studies (Dyment et al., 2015; Koyama et al., 2008), *Gdf5Cre+* cells within and flanking the joint interzone gave rise to most joint tissues over postnatal time, including articular cartilage and intrajoint ligaments (Fig. 4G–L and Fig. S3). *Dkk3-CE+* cells induced at E17.5 elicited similar patterns (Fig. 4Q–T). Interestingly however, *Prg4-CE+* cells induced at E17.5 were

present throughout the entire thickness of articular cartilage at every stage (Fig. 4M–N), but were few in number in ligaments such as the anterior and posterior cruciate ligaments (Fig. 4O–P, arrows) compared to the numerous *Gdf5-CE+* and *Dkk3-CE+* cells (Fig. 4K, S, arrows). The differential distribution of *Prg4-CE+* cells was even more apparent in frontal sections in which articular cartilage and ligaments were present (Fig. S1C). When first induced at P28, *Prg4-CE+* cells populated the top 2–3 layers of articular cartilage at P31 and 2 months (Fig. 4U, V), while *Dkk3-CE+* cells were scanty and limited only to most superficial layer (Fig. 4Y, Z, arrow), in agreement with previous studies on *Dkk3* expression (Lui et al., 2015). Within ligaments, *Prg4-CE+* cells and, to a lesser extent *Dkk3-CE+* cells, were now more conspicuous (Fig. 4W–X, Z'–Z''). The data indicate that around E17.5 the *Gdf5+* cell progeny is routed into articular and ligament fates, with the ligament lineage marked by a *Gdf5+/Dkk3+* character plus a *Scleraxis+/Sox9+* character (Sugimoto et al., 2013) but scanty *Prg4+* character. Waves of *Prg4+* cells are likely generated over time in different joint locations and tissues.

Specific joint progenitor cell populations respond to acute articular cartilage injury

The intrinsic repair capacity of articular cartilage is poor, and studies detecting mesenchymal stem cells in adult synovium and articular cartilage provided clues toward future possible, albeit not yet realized therapeutic repair strategies (Johnstone et al., 2013). Given our data above showing persistence of embryonically-traced cells or their progenies in adult tissues, we asked whether and which of these cells would respond to acute injury (Li et al., 2013). We created a full-thickness osteochondral defect in femoropatellar groove of 2 month-old mice and monitored the acute injury response, this being an established model (Fig. 5A–B, circled area) (Fitzgerald et al., 2008). By day 7 after injury, cells filled the defect (Fig. 5C, dashed line) and the synovium was considerably thicker in operated (Fig. 5C–D, asterisk) than mock-operated mice (Fig. 5A). In about 10% of cases and as seen previously (39), there was evidence of severe synovial metaplasia; interestingly in these cases, synovial tissue was often continuous with cells filling the defect (Fig. 5D, arrowhead), yet appearing unattached to adjacent uninjured articular cartilage (Fig. 5D, arrow).

To investigate the acute responses of embryonically-labeled cells to injury, we created focal osteochondral defects in adult *Prg4-CE/R26-tdTomato* and *Dkk3-CE/R26-zsGreen* mice injected with tamoxifen once at E17.5. By 7 days, there was a marked increase in both *Prg4-CE+* and *Dkk3-CE+* cells, particularly within the thickened synovium (Fig. 5F, H, asterisks) compared to mock-operated controls (Fig. 5E, G, asterisks). Quantification showed that about 70% of synovium cells in operated knees were *Prg4-CE+* and about 35% of them were *Dkk3-CE+* (Fig. 5L, upper histograms). Strikingly, cells seemingly entering and filling the injury site were often not only continuous with synovium but largely *Prg4-CE+* (Fig. 5F, dashed line). In all cases evaluated, including those with lower synovial hyperplasia and those lacking direct contact, both *Prg4-CE+* and *Dkk3-CE+* cells were present within the defect site. There were also *Prg4-CE-* and *Dkk3-CE*-negative cells in the defect reflecting incomplete labeling efficiency or contribution from other cell sources such as subchondral bone. To evaluate contribution of cell proliferation, EdU was administered once after 6 days from surgery, and labeled cells were examined on day 7. Many *Prg4+* cells within both the defect and synovium were co-labeled with EdU (Fig. 5I–J, green color, arrowheads), but

there was little to no incorporation in neighboring articular cells (Fig. 5K–L, arrowhead), indicating that proliferating *Prg4-CE+* cells within synovium -but not adjacent articular cartilage- likely gave rise to cells present within defect site.

The above experiments were repeated in *Prg4*-CE mice after tamoxifen administration at P28, a stage in which *Prg4-CE+* cells were confined to upper articular cartilage layers and synovial lining (Fig. 6A, arrow and arrowhead, respectively). We observed similar exuberant increases in *Prg4-CE+* cells within synovium (Fig. 6C, asterisk) but not cartilage itself (Fig. 6C, arrows), and similar patterns of apparent cell invasion into the defects (Figure 6C, dashed line). Because subchondral bone was not labeled by tamoxifen injection at P28, the invading cells were likely of synovial origin. To verify this finding, we evaluated *Gdf5Cre/R26-Confetti* mice 7 days after surgery, and saw no obvious migration of same color labeled cells into the defect from adjacent articular cartilage (Fig. S6B, arrows).

To distinguish cell progeny from newly-emerging cells, we examined defects in 2 month-old *Prg4-CE/R26-zsGreen/Prg4mCherry* reporter mice injected with tamoxifen at P28 (Decker et al., 2014a). While numerous *Prg4-CE+* (green-colored) cells occupied the enlarged synovium (Fig. 6D, asterisk) and defect site (Fig. 6D, dashed line) and few such cells were present in controls (Fig. 6B), real-time *Prg4mCherry* expressing (red-colored) cells were largely restricted to synovial lining and articular surface eliciting some degree of co-expression (Fig. 6D, yellow color). Thus, while cells within the defect site were largely derived from those with a *Prg4-CE* lineage, *Prg4* itself was not actively expressed by day 7 post-surgery.

Recent studies have suggested that specific mesenchymal stem cell (MSC) niches reside within knee joint synovium, including populations of slow-cycling cells expressing CD44 and P75 that are established markers of multipotency (Kurth et al., 2011). In uninjured knees, *Prg4-CE+* synovial lining cells were CD44-positive (Fig. 6E, arrowhead) and those in both lining and sub-synovial tissues were often P75-positive (Fig. 6F, arrowhead). At day 7 post-surgery, proliferating *Prg4-CE+* cells throughout the synovium and defect site displayed strong CD44 and P75 staining (Fig. 6G–J), thereby indicating that many were mesenchymal in character and synovial in origin.

Discussion

Our data provide new insights into limb synovial joint development, growth and morphogenesis and a better understanding of how articular cartilage attains its unique and stratified organization over postnatal time. Rather than being solely driven by apposition of daughter cells from surface to deep zone to create columns (Kozhemyakina et al., 2015), our data indicate that articular cartilage mainly relies on changes in cell distribution and volume to create cellular stacks spanning its vertical axis and achieve its functional and mature thickness within the central region of the knee (see model in Figure 7). Because the stacks are not entirely made of daughter cells (see Li et al, 2016 for similar data) and do not contain perfectly aligned cells such as those present in growth plate, they likely develop via lateral rearrangement and realignment of neighboring cells and small groups. This process could be driven by mechanisms such as cell intercalation by convergent extension, which permits

tissue growth and elongation with minimal to no proliferation (Tada and Heisenberg, 2012). A major mechanism regulating cell intercalation is the planar cell polarity (PCP) pathway, and PCP components such as *Vangl2* and *Ror2* were in fact found to regulate alignment of incipient chondrocytes along the proximo-distal axis in early limb patterning (Gao et al., 2011). The process could also be promoted by indirect mechanisms such as changes in deposition of collagen fibrils that as shown here, go from being isotropic and random to anisotropic and vertically oriented with age, paralleling the formation of cell stacks.

There has been a great of interest regarding the proliferative capacity and apoptotic processes occurring during limb joint development (Decker et al., 2014b). It was originally suggested that joint cavitation at embryonic stages is due to cell death locally occurring along the cavitation boundary (Abu-Hijleh et al., 1997; Kimura and Shiota, 1996), but subsequent studies did not confirm those findings (Ito and Kida, 2000). This agrees with our TUNEL staining data showing minimal, if any, cell death at neonatal and juvenile stages. The conspicuous positive TUNEL staining we observe in adults, particularly in the deep articular zones (Fig. 3), may be due to tissue remodeling and joint structure consolidation, but more work will be needed to assess roles and relevance. With regard to proliferation, our data confirm that there is strong mitotic activity at early stages of joint development (Candela et al., 2014; Li et al., 2016; Ray et al., 2015), but proliferation then dwindles and decreases markedly by 1 to 2 months of age, characterizing about 3% of the overall cell population. This is in contrast to the high rates of proliferation previously observed in mouse tibia articular cells at P28 in which about 70% of superficial cells and a significant number of deep zone cells had incorporated EdU (Kozhemyakina et al., 2015). We do not know what could be the basis of such markedly discordant observations. One possibility is that unlike our mice with a full complement of *Prg4* genes, the knock-in *Prg4-CreER* mice used in that study were heterozygous null for *Prg4* and such deficiency may have caused higher joint tissue turnover –and hence higher cell proliferation- because of reduced lubrication and increased friction. We should point out that as the epiphyses of long bones grow and greatly expand laterally over postnatal age, articular cartilage needs to expand laterally as well to continue to fully cover the epiphyseal end of long bones. It is thus possible that additional and actively proliferating progenitors may be recruited from lateral sites to sustain postnatal epiphyseal expansion through adulthood, and preliminary data indicate that cells near or within the groove of Ranvier may be involved in such task (not shown) (Decker et al., 2014b, 2015). Thus, cell proliferation and cell death appear to be spatially restricted processes and distinctly characterize the successive stages of joint development, growth and expansion from neonatal to adult stages.

By being the first overt sign of incipient limb joint formation, the mesenchymal interzone has long attracted a great deal of attention (Holder, 1977). Because it emerges at the site previously occupied by chondrocytes within uninterrupted cartilaginous skeletal anlagen in early limbs, its cells were proposed to descend from de-differentiated chondrocytes (Craig et al., 1987; Nalin et al., 1995). Such chondrocyte-to-interzone cell relationship and lineage continuity were substantiated by genetic tracing of *Sox9+* and *Dcx+* cell progenies (Soeda et al., 2010; Zhang et al., 2010). Interestingly however, the quintessential interzone marker *Gdf5* is expressed not only by interzone cells anatomically in line with the cartilaginous anlagen, but also mesenchymal cells flanking joint sites (Decker et al., 2015) (Fig. S3).

Thus, the “interzone” may have a dual origin (see model in Fig. 7), with centrally located cells being direct descendants of chondrocytes and with flanking cells deriving from surrounding mesenchyme as we originally showed by DiI injection in chick embryo limbs and labeled cell distribution over developmental time (Pacifici et al., 2006). This is in line with data indicating that *Tgfbr2+* cells serve as a subset of joint site-associated cells with specific developmental roles and fate (Li et al., 2013). Unlike the original *Gdf5Cre* mice that trace the entire interzone (Fig. 4 and Fig. S7) (Rountree et al., 2004), our new *Gdf5-CE* line is not only inducible but less efficient compared to *Gdf5Cre* (Fig. 4 and Fig. S3), allowing us to trace and track subsets of developing interzone-associated cells. Our data show that cells labeled by tamoxifen injection at E13.5 are restricted to the outer mesenchymal perimeter of incipient digit joints, remain in those locations over prenatal and postnatal time and participate in formation of local differentiated tissues, including synovial lining and inner capsule. These cells could be part of the flanking cell population recruited into the *Gdf5+* lineage. Distinct sub-populations of *Gdf5Cre+* cells were observed in a recent study in which cells were labeled at successive embryonic times and collected at E18.5 (Shwartz et al., 2016). The authors proposed that waves of *Gdf5*-negative, *Sox9*-positive and *Col2a1*-negative progenitors migrate into, and give rise to, the interzone, then express *Gdf5* and produce joint tissues. Notably and as our data indicate, onset, timing and location of *Gdf5* expression may indeed play a key role in lineage divergence and generation of distinct joint tissues. Taken together, the data lead to the tantalizing and important conclusion that while interzone cells share a *Gdf5+* character, they have or acquire diverse developmental programs and follow local differentiation paths and fates over time, possibly aided by positional cues.

Prg4 is a complex gene whose products include lubricin, superficial zone protein (SZP), megakaryocyte-stimulating factor (MSF) and hemangiopoietin (HAPO) (Jay et al., 2001; Jones and Flannery, 2007). These products result from alternative splicing and post-translational modifications and are likely to have distinct function. Because of their mucin-rich domain, lubricin and SPZ are thought to provide boundary lubrication and unhindered joint motion, although this role may primarily be due to phospholipids and hyaluronan interacting with cell surface-bound lubricin (Seror et al., 2015). Our rtPCR data show that several *Prg4* transcripts are expressed in P0 knee joints, with each variant lacking different exon combinations (see Fig. S1G). We do not know whether the various *Prg4-CE+* populations present in developing, growing and adult joint tissues express different *Prg4* variants, whether such expression patterns change over time, and what function each variant could have. What is abundantly clear from our data is that synovium-associated *Prg4-CE+* cells traced at E17.5 or P28 are exquisitely sensitive to joint injury and respond massively to it, while neighboring *Prg4-CE+* cells within articular cartilage itself appear to be remarkably passive and fail to mobilize, at least within the acute time frame studied here. This is reminiscent of the lack of chondrocyte mobilization observed during axolotl limb repair and regeneration (Currie et al., 2016). Thus, different *Prg4-CE+* populations seem to differ in responsiveness, sensitivity and function, and those in synovium may exert a pioneer function in acute injury response. The synovium has long been recognized as an integral source of cells contributing to cartilage repair (Kurth et al., 2011), and tools to target synovium-

associated *Prg4-CE+* cells or inclusion of these cells in bioengineered constructs could offer novel and effective therapies to boost repair and regeneration of joint tissues.

Supplementary Material

Refer to Web version on PubMed Central for supplementary material.

Acknowledgments

We thank Ms. Angelique Thornton for assistance with mouse maintenance and experiments. We would like to express our gratitude to the Reviewers for their constructive criticisms, pointed questions and many suggestions that have allowed us to improve the manuscript significantly.

Funding

This study was supported by NIAMS grant F32AR064071 to R.S.D; NIAMS grants AR062908 to M.P. and M.E.I. and AR060899 to P.M.; and NIH grant S10 RR027128 to the PennVet Imaging Core Facility.

References

Abu-Hijleh G, Reid O, Scothorne RJ. Cell death in the developing chick knee joint. I. Spatial and temporal patterns. Clin. Anat. 1997; 10:183–200. [PubMed: 9135886]

Archer CW, , Caterson B, , Benjamin M, , Ralphs JR. The Biology of the Synovial Joint Harwood Academics; London: 1999

Caldwell KL, Wang J. Cell-based articular cartilage repair: the link between development and regeneration. Osteoarthr. Cart. 2015; 23:351–362.

Candela ME, Cantley L, Yasuhara R, Iwamoto M, Pacifici M, Enomoto-Iwamoto M. Distribution of slow-cycling cells in epiphyseal cartilage and requirement of β-catenin signaling for their maintenance in growth plate. J. Ortho. Res. 2014; 32:661–668.

Craig FM, Bentley G, Archer CW. The spatial and temporal pattern of collagens I and II and keratan sulphate in the developing chick metatarsophalangeal joint. Development. 1987; 99:383–391. [PubMed: 2958266]

Currie JD, Kawaguchi A, Moreno Traspas R, Schuez M, Chara O, Tanaka EM. Live imaging of axolotl digit regeneration reveals spatiotemporal choreography of diverse connective tissue progenitor pools. Dev. Cell. 2016; 39:411–423. [PubMed: 27840105]

Decker RS, Koyama E, Enomoto-Iwamoto M, Maye P, Rowe P, Zhu S, Schultz PG, Pacifici M. Mouse limb skeletal growth and synovial joint development are coordinately enhanced by Kartogenin. Dev. Biol. 2014a; 395:255–267. [PubMed: 25238962]

Decker RS, Koyama E, Pacifici M. Genesis and morphogenesis of limb synovial joints and articular cartilage. Matrix Biol. 2014b; 39:5–10. [PubMed: 25172830]

Decker RS, Koyama E, Pacifici M. Articular cartilage: structural and developmental intricacies and questions. Curr. Osteoporos. Rep. 2015; 13:407–414. [PubMed: 26408155]

Dowthwaite GP, Bishop JC, Redman SN, Khan IM, Rooney P, Evans DJR, Haughton L, Bayram Z, Boyer S, Thomson B, Wolfe MS, Archer CW. The surface of articular cartilage contains a progenitor cell population. J. Cell Sci. 2003; 117:889–897.

Dyment NA, Breidenbach AP, Schwartz AG, Russell RP, Aschbacher-Smith L, Liu H, Hagiwara Y, Jiang R, Thomopoulos S, Butler DL, Rowe DW. Gdf5 progenitors give rise to fibrocartilage cells that mineralize via hedgehog signaling to form the zonal enthesis. Dev. Biol. 2015; 405:96–107. [PubMed: 26141957]

Fitzgerald J, Rich C, Burkhardt D, Allen J, Herzka AS, Little CB. Evidence for articular cartilage regeneration in MRL/Mpj mice. Osteoarthr. Cart. 2008; 16:1319–1326.

Gannon AR, Nagel T, Bell AP, Avery NC, Kelly DJ. Postnatal changes to the mechanical properties of articular cartilage are driven by the evolution of its collagen network. Eur. Cells Mater. 2015; 29:105–121.

Gao B, Song H, Bishop K, Elliot G, Garrett L, English MA, Andre P, Robinson J, Sood R, Minami Y, Economides AN, Yang Y. Wnt signaling gradients establish planar cell polarity by inducing Vangl2 phosphorylation through Ror2. Dev. Cell. 2011; 20:163–176. [PubMed: 21316585]

Ginzberg MB, Kafri R, Kirschner M. On being the right (cell) size. Science. 2015; 348:1245075. [PubMed: 25977557]

Gong S, Kus L, Heintz N. Rapid bacterial artificial chromosome modification for large-scale mouse transgenesis. Nat. Protocols. 2010; 5:1678–1696. [PubMed: 20885380]

Holder N. An experimental investigation into the early development of the chick elbow joint. J. Embryol. Exp. Morphol. 1977; 39:115–127. [PubMed: 886251]

Huey DJ, Hu JC, Athanasiou KA. Unlike bone, cartilage regeneration remains elusive. Science. 2012; 338:917–921. [PubMed: 23161992]

Hughes LC, Archer CW, ap Gwynn I. The ultrastructure of mouse articular cartilage: collagen orientation and implications for tissue functionality. A polarised light and scanning electron microscope study and review. Eur. Cells Mater. 2005; 9:68–84.

Hunziker EB, Kapfinger E, Geiss MD. The structural architecture of adult mammalian articular cartilage evolves by a synchronized process of tissue resorption and neoformation during postnatal development. Osteoarthr. Cart. 2007; 15:403–413.

Hyde G, Dover S, Aszodi A, Wallis GA, Boot-Handford RP. Lineage tracing using matrilin-1 gene expression reveals that articular chondrocytes exist as the joint interzone forms. Dev. Biol. 2007; 304:825–833. [PubMed: 17313942]

Ito MM, Kida MY. Morphological and biochemical re-evaluation of the process of cavitation in the rat knee joint: cellular and cell strata alterations in the interzone. J. Anat. 2000; 197:659–679. [PubMed: 11197539]

Iwamoto M, Tamamura Y, Koyama E, Komori T, Takeshita N, Williams JA, Nakamura T, Enomoto-Iwamoto M, Pacifici M. Transcription factor ERG and joint and articular cartilage formation during mouse limb and spine skeletogenesis. Dev. Biol. 2007; 305:40–51. [PubMed: 17336282]

Jay GD, Tantravahi U, Britt DE, Barrach HJ, Cha CJ. Homology of lubricin and superficial zone protein (SZP): products of megakaryocyte stimulating factor (MSF) gene expression by human synovial fibroblasts and articular chondrocytes localized to chromosome 1q25. J. Orthop. Res. 2001; 19:677–687. [PubMed: 11518279]

Jenner F, Ijpma A, Cleary MA, Heijsman D, Narcis R, van der Spek PJ, Kremer A, van Weeren R, Brama P, van Osch GJ. Differential gene expression of the intermediate and outer interzone layers of developing articular cartilage in murine embryos. Stem Cells Dev. 2014; 23:1883–1898. [PubMed: 24738827]

Johnstone B, Alini M, Cucchiarini M, Dodge GR, Eglin D, Guilak F, Madry H, Mata A, Mauck RL, Semino CE, Stoddart MJ. Tissue engineering for articular cartilage repair. The state of the art. Eur. Cells Mater. 2013; 25:248–267.

Jones ARC, Flannery CR. Bioregulation of lubricin expression by growth factors and cytokines. Eur. Cells Materials. 2007; 13:40–45.

Julkunen P, Harijula T, iivarinen J, Marjanen J, Seppanen K, Narhi T, Arokoski J, Lammi MJ, Brama PA, Jurvelin JS, Helminen HJ. Biomechanical, biochemical and structural correlations in immature and mature rabbit articular cartilage. Osteoarthr. Cart. 2009; 17:1628–1638.

Kawamoto T, Kawamoto K. Preparation of thin frozen sections from nonfixed and undecalcified hard tissues using Kawamot's film method (2012). Methods Mol. Biol. 2014; 1130:149–164. [PubMed: 24482171]

Kimura S, Shiota K. Sequential changes of programmed cell death in developing fetal mouse limbs and its possible roles in limb morphogenesis. J. Morphol. 1996; 229:337–346. [PubMed: 8765811]

Koyama E, Shibukawa Y, Nagayama M, Sugito H, Young B, Yuasa T, Okabe T, Ochiai T, Kamiya N, Rountree RB, Kingsley DM, Iwamoto M, Enomoto-Iwamoto M, Pacifici M. A distinct cohort of progenitor cells participates in synovial joint and articular cartilage formation during mouse limb skeletogenesis. Dev. Biol. 2008; 316:62–73. [PubMed: 18295755]

Kozhemyakina E, Zhang MQ, Ionescu A, Kobayashi A, Kronenberg HM, Warman ML, Lassar AB. Identification of a Prg4-expressing articular cartilage progenitor cell population in mice. Arthr. Rheum. 2015; 67:1261–1273.

Kurth TB, Dell' Accio F, Crouch V, Augelio A, Sharpe PT, De Bari C. Functional mesenchymal stem cell niches in adult mouse knee joint synovium in vivo. Arthr. Rheum. 2011; 63:1289–1300. [PubMed: 21538315]

Li L, Newton PT, Bouderlique T, ejnohova M, Zikmund T, Kozhemyakina E, Xie M, Krivanek J, Kaiser J, Qian H, Dyachuk V, Lassar AB, Warman ML, Barenius B, Adameyko I, Chagin AS. Superficial cells are self-renewing chondrocyte progenitors, which form the articular cartilage in juvenile mice. FASEB J. 2016; 31:1067–1084. [PubMed: 27965322]

Li TF, Longobardi L, Myers TJ, Temple JD, Chandler RL, Ozkan H, Contaldo C, Spagnoli A. Joint TGF-β type II receptor-expressing cells: ontogeny and characterization as joint progenitors. Stem Cells Dev. 2013; 22:1342–1359. [PubMed: 23231014]

Lui JC, Chau M, Chen W, Cheung CS, Hanson J, Rodriguez-Canales J, Nilsson O, Baron J. Spatial regulation of gene expression during growth of articular cartilage in juvenile mice. Pediatr. Res. 2015; 2015:406–415.

Mow VC, Ratcliffe A, Poole AR. Cartilage and diartrodial joints as paradigms for hierarchical materials and structures. Biomaterials. 1992; 13:67–97. [PubMed: 1550898]

Mow VC, , Sugalski MT. Physiology of synovial joints and articular cartilage. In: Gonzales EG, editorPhysiological Basis of Rehabilitation Medicine 3. Butterworth Heinemann Pubs; Boston: 2001 133168

Nalin AM, Greenlee TK, Sandell LJ. Collagen gene expression during development of avian synovial joints: transient expression of type II and XI collagen genes in the joint capsule. Dev. Dyn. 1995; 203:352–362. [PubMed: 8589432]

Pacifici M, Koyama E, Shibukawa Y, Wu C, Tamamura Y, Enomoto-Iwamoto M, Iwamoto M. Cellular and molecular mechanisms of synovial joint and articular cartilage formation. Ann. N.Y. Acad. Sci. 2006; 1068:74–86. [PubMed: 16831907]

Ray A, Ingh PNP, Sohaskey ML, Harland RM, Bandyopadhyay A. Precise spatial restriction of BMP signaling is essential for articular cartilage differentiation. Development. 2015; 142:1169–1179. [PubMed: 25758226]

Rhee DK, Marcelino J, Baker M, Gong Y, Smits P, Lefebvre V, Jay GD, Stewart M, Wang H, Warman ML, Carpten JD. The secreted glycoprotein lubricin protects cartilage surfaces and inhibits synovial cell outgrowth. J. Clin. Invest. 2005; 115:622–631. [PubMed: 15719068]

Rountree RB, Schoor M, Chen H, Marks ME, Harley V, Mishina Y, Kingsley DM. BMP receptor signaling is required for postnatal maintenance of articular cartilage. PLoS Biology. 2004; 2:1815–1827.

Seror J, Zhu L, Goldberg R, Day AJ, Klein J. Supramolecular synergy in the boundary lubrication of synovial joints. Nat. Communications. 2015; 6:6497.

Shwartz Y, Viukov S, Krief S, Zelzer E. Joint development involves a continuous influx of Gdf5-positive cells. Cell Reports. 2016; 15:1–11. [PubMed: 27052168]

Snippert HJ, van der Flier LG, Sato T, van Es JH, van der Born M, Kroon-Veeboer C, Barker N, Klein AM, van Rheenen J, Simons BD, Clevers H. Intestinal crypt homeostasis results from neutral competition between symmetrically dividing Lgr5 stem cells. Cell. 2010; 143:134–144. [PubMed: 20887898]

Soeda T, Deng JM, de Crombrugghe B, Behringer RR, Nakamura T, Akiyama H. Sox9-expressing precursors are the cellular origin of the cruciate ligament of the knee joint and the limb tendons. Genesis. 2010; 48:635–644. [PubMed: 20806356]

Sugimoto Y, Takimoto A, Akiyama H, Kist R, Scherer G, Nakamura T, Hiraki Y, Shukunami C. Scx+/Sox9+ pprogenitors contribute to the establishment of the junction between cartilage and tendon/ligament. Development. 2013; 140:2280–2288. [PubMed: 23615282]

Tada M, Heisenberg C-P. Convergent extension: using collective cell migration and cell intercalation to shape embryos. Development. 2012; 139:3897–3904. [PubMed: 23048180]

Williams R, Khan IM, Richardson K, Nelson I, McCarthy HE, Analbelsi T, et al. Identification and clonal characterirization of a progenitor cell sub-population in normal human articular cartilage. PLoS One. 2010; 5:e13246. [PubMed: 20976230]

Witte F, Dokas J, Neuendorf F, Mundlos S, Stricker S. Comprehensive expression analysis of all Wnt genes and their major secreted antagonists during mouse limb development and cartilage differentiation. Gene Exp. Patterns. 2009; 9:215–223.

Youn I, Choi JB, Cao L, Setton LA, Guilak F. Zonal variations in the three-dimensional morphology of the chondron measured in situ using confocal microscopy. Osteoarthr. Cart. 2006; 14:889–897.

Zhang Q, Cigan AD, Marrero L, Lopreore C, Liu S, Ge D, Savoie FH, You Z. Expression of doublecortin reveals articular chondrocyte lineage in mouse embryonic limbs. Genesis. 2010; 49:75–82.

Highlights

- Local progenitor cells emerging at distinct sites and times give rise to distinct joint tissues
- Articular cartilage zonal structure mainly reflects cell rearrangement into stacks
- Postnatal cartilage thickening is driven by zonal-specific increases in cell volume
- Synovial progenitors with a Prg4 lineage signature appear exquisitely responsive to tissue injury

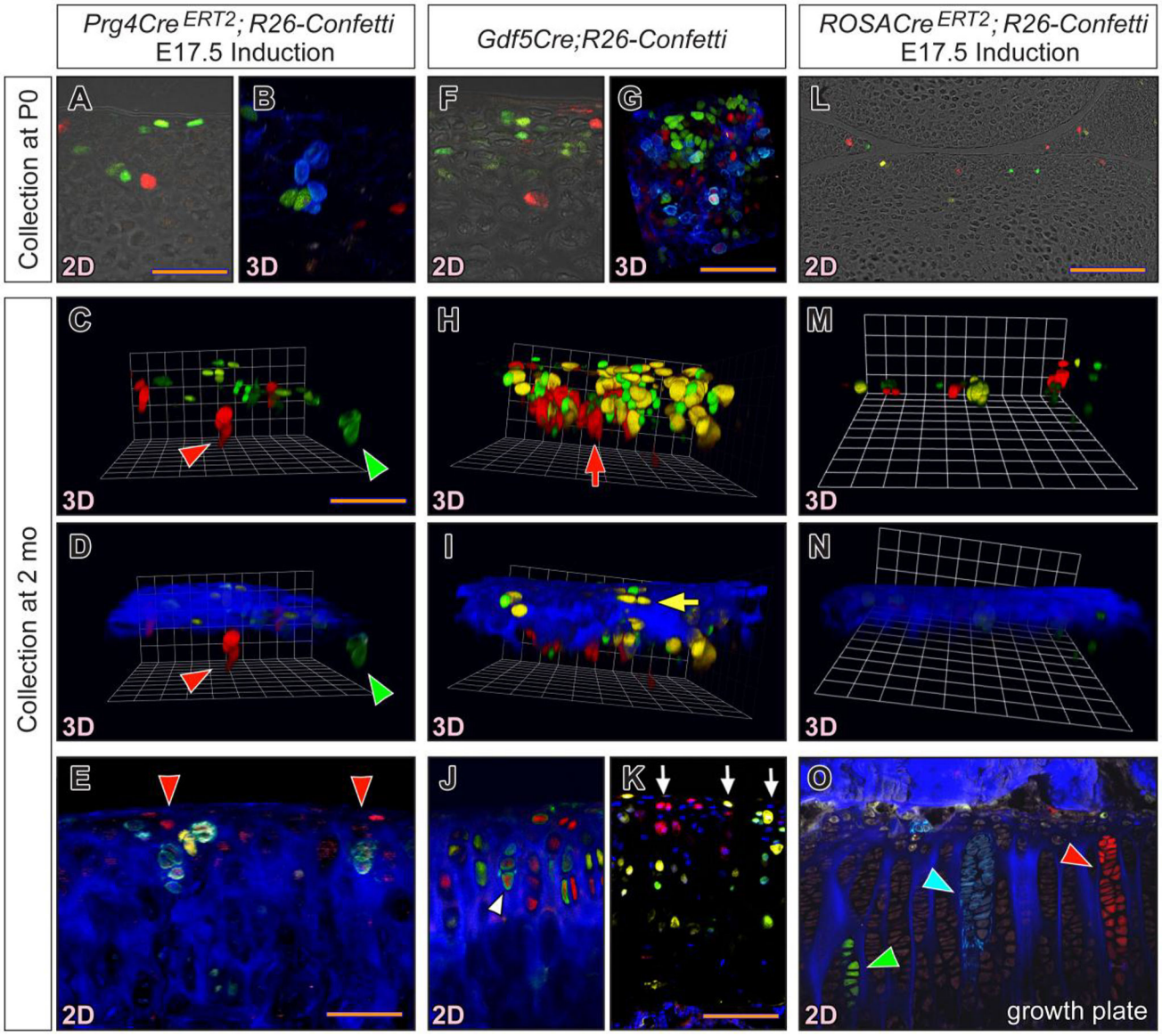

Fig. 1.

Postnatal articular cartilage development and growth involve formation of non-daughter cell stacks. (**A–E**) Two-dimensional (2D) sections and 3D fluorescence images of joints from *Prg4*-CE*/R26-Confetti* mice induced with tamoxifen at E17.5 and collected at: P0 (newborn) **(A–B)** and 2 months of age **(C–E)**. **D** is the same 3D image in **C**, but with superimposed second harmonic signal from matrix (blue color). Arrows in **D** indicate local same-color reporter clusters throughout the tissue. Arrows in **E** indicate non-daughter cells in stack expressing different reporters. (**F–K**) 2D and 3D fluorescence images of joints from constitutive *Gdf5Cre/Confetti* mice at: P0 **(F–G)**; and 2 months of age **(H–K)**. **I** is the same 3D image in **H**, but with superimposed second harmonic signal (blue color). Red arrow in **H** indicates clonal expansion perpendicular to the articular surface, while yellow arrow in **I** indicates clonal expansion parallel to the articular surface. Arrowhead in **J** points to occasional dual reporter-positive cell; arrows in **K** point to examples of non-daughter cell

stacks. (**L–O**) 2D and 3D images of joints from *ROSA*-CE*/R26-Confetti* mice induced with tamoxifen at E17.5 and examined at: P0 **(L)**; and 2 months **(M–O)**. (**O**) Fluorescence image of proximal tibia growth plate from 1 month-old *ROSA-CE/R26-Confetti* mice induced at E17.5. Arrowheads indicate continuous single reporter-expressing chondrocyte columns made of daughter cells. At least 5 mice were evaluated at each stage. A–B and F–G, scale bar = 50 μm; C–D, H–I and M–N, scale bar = 55 μm; E, J, scale bar = 60 μm; K, scale bar = 40 μm; and L, scale bar = 125 μm.

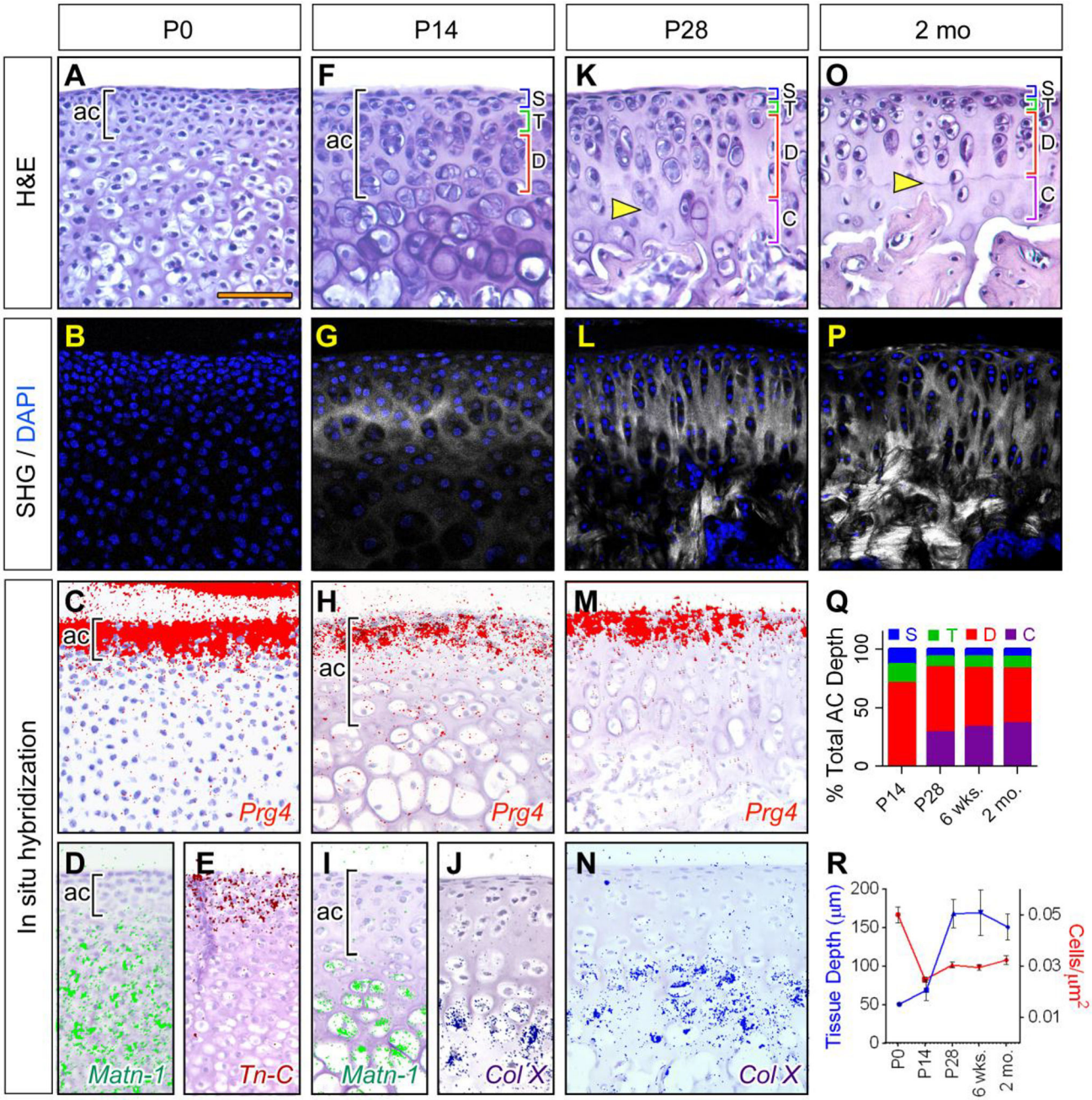

Fig. 2.

Zonal arrangement and thickening of articular cartilage are linked to changes in cellularity and collagen matrix configuration. (**A–E**) Incipient proximal tibia articular cartilage at P0 consists of small and closely-bound cells (**A**, bracket) that express *Prg4* (**C**) and *TnC* (**E**), but lack *Matn1* expression **(E)** and a SHG-detectable collagen matrix (**B**). Brackets demarcate the approximate thickness of incipient articular cartilage which overlays *Matn1*-expressing shaft cartilage destined for secondary ossification (**D**). (**F–J**) Articular cartilage at P14 is thicker (**F**, bracket). Its surface zone (S) retains *Prg4* expression **(H)**, while its developing transitional (T) and deep (D) zones display isotropic SHG-detectable collagen

fibrils (**G**). Strong *Matn1* and *ColX* expression depicts underlying secondary ossification center cartilage (**I–J**). (**K–P**) At P28 and 2 months, articular cartilage acquires typical zones that include a narrow surface *Prg4*-expressing zone (**M**) and intermediate and deep zones with chondrocyte stacks with anisotropic collagen matrix (**L** and **P**) with underlying subchondral *ColX* expressing cells **(N)**. A characteristic tidemark delineates the boundary between deep and calcified zones (**K** and **O**, arrowheads). Data are representative of a minimum of 6 mice evaluated at each stage. (**Q**) Relative sizes of superficial (S), transitional (T), deep (D) and calcified (C) zones at P14, P28, 6 weeks and 2 months were calculated by histological morphometry; n=12 for each time point. (**R**) Cellularity (right Y axis, red line) versus overall tissue thickness (left Y axis, blue line) from P0 to 2 months were determined by fluorescence microscopy and histomorphometry; n=12 for each time point, mean ± s.d.. Images A–P same scale, bar in A = 75 μm.

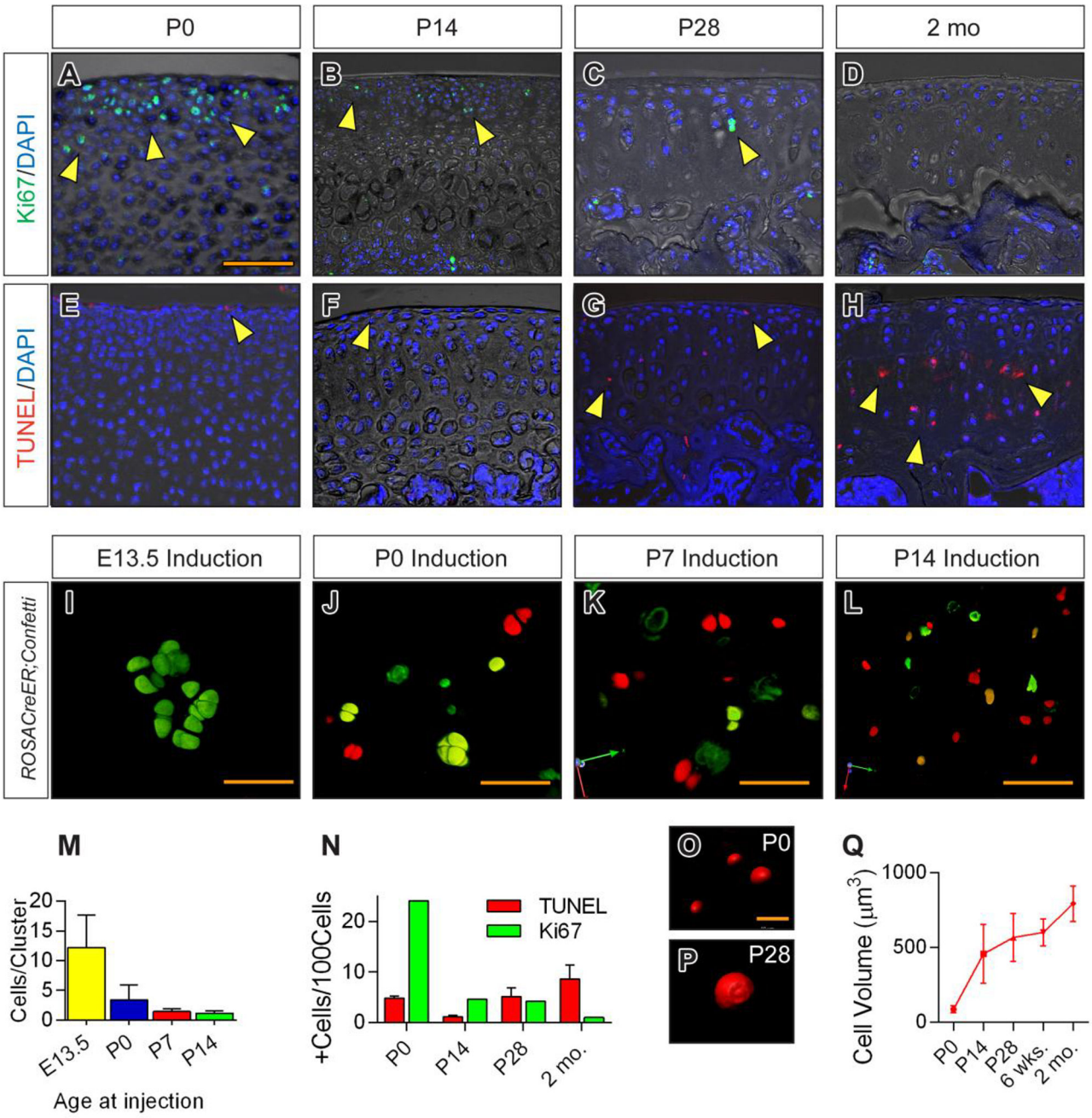

Fig. 3.

Differential changes in cell proliferation, death and volume subtend tibial articular cartilage growth over age. (**A–H**) Immunostaining fluorescence images of cell proliferation marker Ki67 (**A–D**) and TUNEL staining for apoptosis (**E–H**) indicating that proliferation was maximal at early stages while cell death was maximal at late stages. Arrowheads point to representative positive cells. (**I–L**) Cell progeny clusters in articular tissue in *ROSA*-CE/*R26-Confetti* mice induced once at E13.5, P0, P7 and P14 and examined at 2 months. Images are representative of a minimum of 6 mice evaluated at each stage. Maximal cluster sizes of about 18 cells were observed after E13.5 induction (**I**), and average sizes dwindled

thereafter (**J–L**). (**M–P**) 2D and 3D imaging-based quantifications of: average cell cluster size (**M**); Ki67- and TUNEL-positive cell numbers (**N**); individual cells for volume quantification (**O, P**); and calculated average cell volumes (**Q**) at indicated ages. n=4 mice, minimum of 40 cells measured per mouse at each stage. When present, vertical bars indicate means ± s.d. A–E, bar = 75 μm; I–J, bar = 50 μm; K, bar = 60 μm; L, bar =75 μm; and O–P, bar =8 μm.

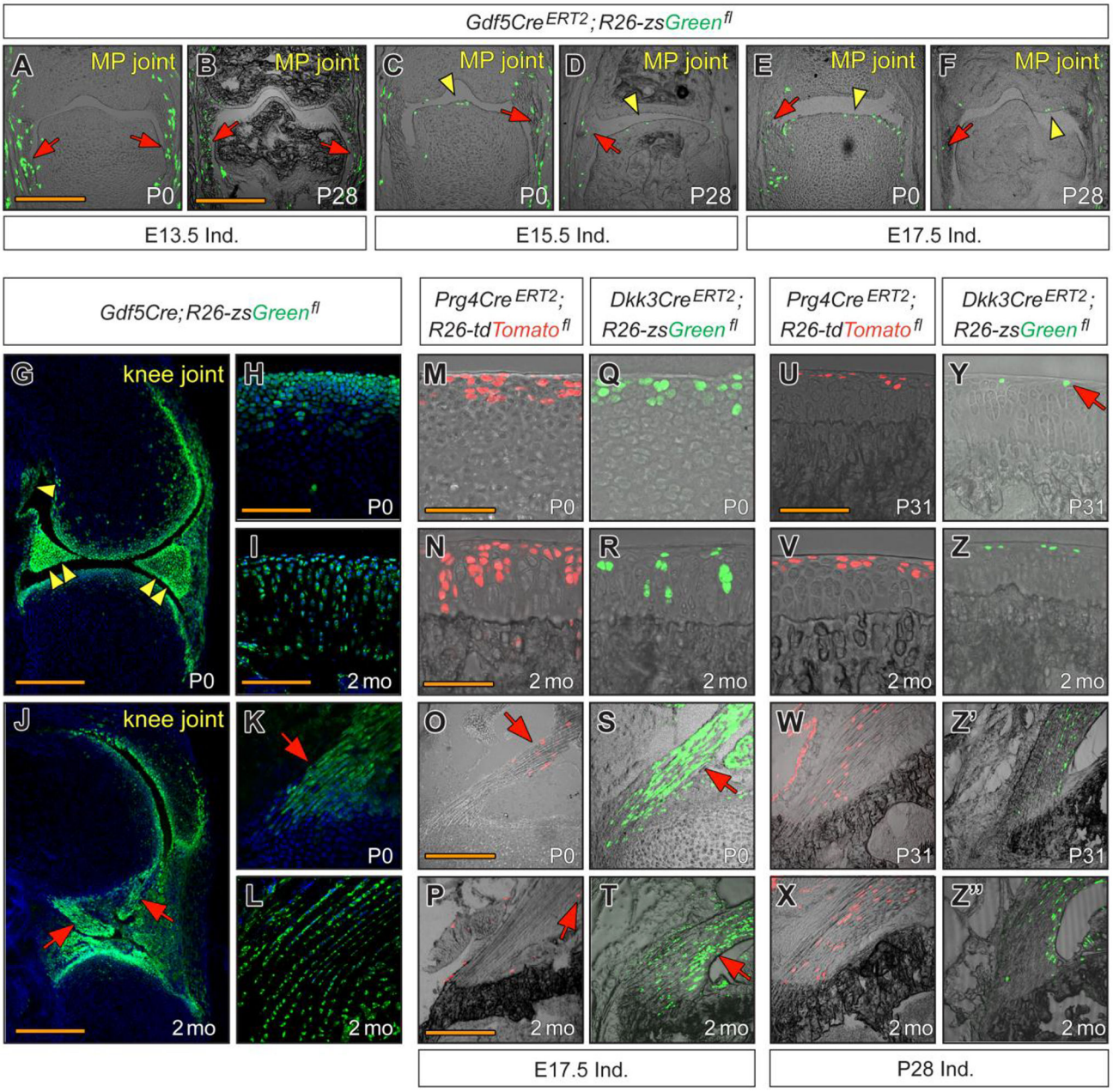

Fig. 4.

Joint progenitors are topographically static and contribute to diverse tissues over developmental time. (**A–F**) Metatarsal-phalangeal joints at P0 (**A, C, E**) and 1 month of age (**B, D, F**) from *Gdf5*-ER*/R26-zsGreen* mice induced once with tamoxifen at E13.5 (**A–B**), E15.5 (**C–D**) or E17.5 (**E–F**) show persistent local distribution of reporter-positive cells over time. Red arrows indicate representative labeled cells in peripheral tissues, and yellow arrowheads indicated representative labeled articular cells. (**G–L**) Images of knee sections from constitutive *Gdf5Cre/GFP* mice indicating that *Gdf5Cre+* cells constitute most joint tissues over indicated times, including ligaments (arrows), meniscus (double arrowheads) and synovium (arrowhead). (**M–T**) Knee joint images showing that both *Prg4-CE+* and

Dkk-CE+ cells in mice induced at E17.5 are present and abundant in tibial articular cartilage at P0 and 2 months (**M–N, Q–R**). *Dkk-CE+* cells are also numerous in posterior cruciate ligament at either age (**S–T**, arrows), whereas *Prg4-CE+* cells are scarce (**O–P**, arrows). Note that *Gdf5Cre+* cells also are abundant in ligaments (**K**, arrow). (**U–Z’’**) In mice induced at P28, *Prg4-CE+* cells populate the surface layers of articular cartilage at P31 and 2 months **(U–V)**, while *Dkk-CE+* cells are rare and only found in the most superficial articular layer (**Y–Z**, arrow). *Prg4-CE+* and *Dkk3-CE+* cells are found throughout the posterior cruciate ligament (**W–X, Z’–Z’’**) at both P31 and 2 months. Images are representative of a minimum of 3 mice evaluated at each stage. Images A, C, E, bar = 75 μm; B, D, F, bar = 125 μm; G, J, bar = 300 μm; and H–Z’’, bar = 100 μm.

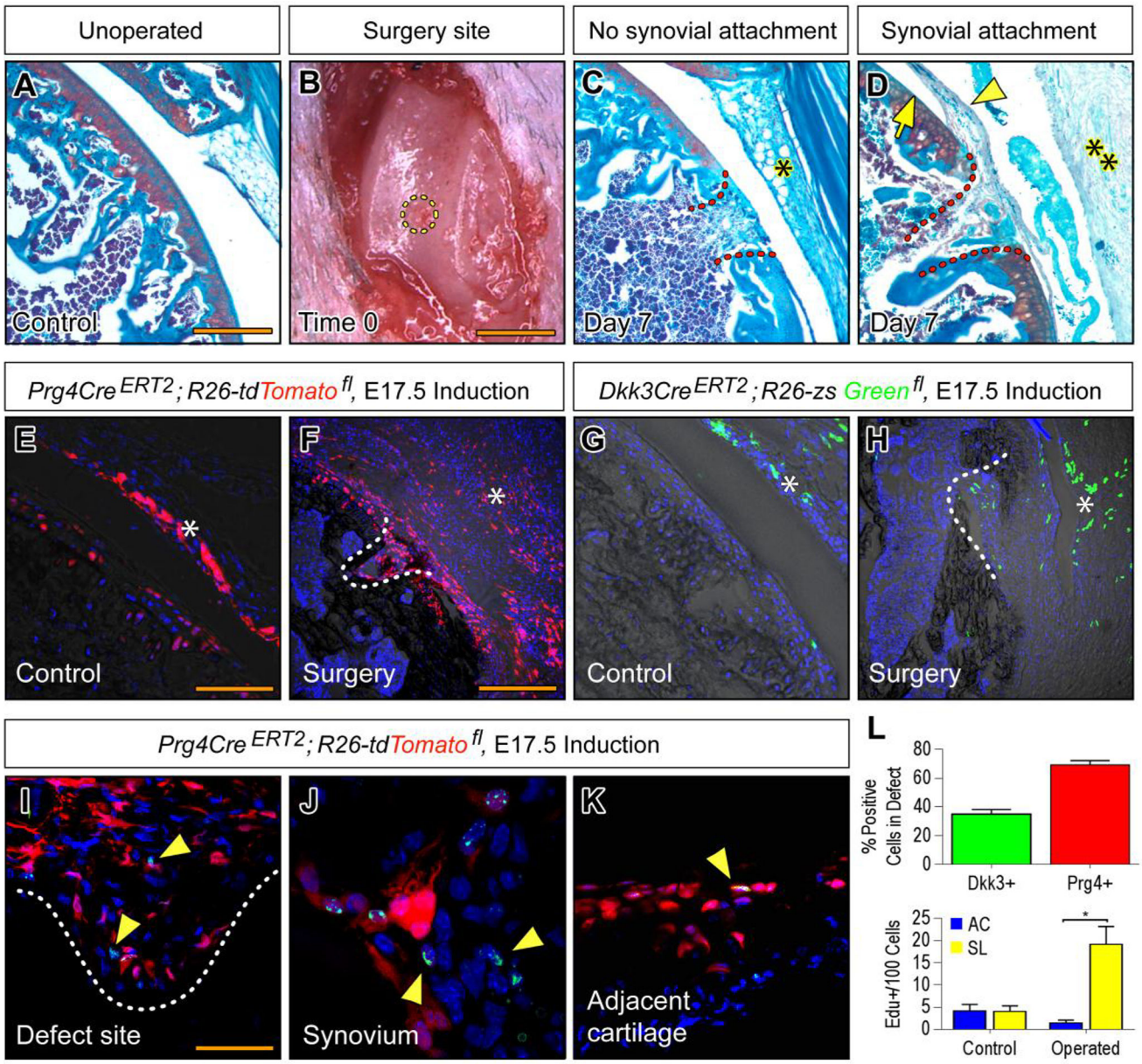

Fig. 5.

Embryonically labeled joint cell populations respond to articular cartilage injury. (**A–D**) Safranin-O histological and anatomical images from un-operated and operated 2 month-old adult knee joints and femoropatellar groove showing: typical joint organization in controls (**A**); operated site immediately after surgery (**B**, circled area); representative field showing minor synovial hyperplasia 7 days after surgery (**C**, asterisk); and more severe synovial hyperplasia after surgery (**D**, double asterisk). Note that cells usually filled the surgical defect by day 7 (**C**, dashed line), and the hyperplastic synovial tissue was often continuous with cells filling the defect (arrowhead), yet appearing unattached to the adjacent articular cartilage (arrow) **(D)**. (**E–H**) In adult mice that were induced with tamoxifen at E17.5, *Prg4-CE+* and *Dkk3-CE+* cells become very numerous within the thickened synovium by day 7 from surgery (**F, H**, asterisks), but remain few in number and restricted to articular and

synovial surfaces in companion controls (**E, G**, asterisks). (**I–K**) EdU labeling (green label) revealed that proliferating cells are present within defect site and synovium (**I–J**), but are rare in adjacent articular cartilage after surgery (**K**, arrow). Images are representative of a minimum of 6 mice evaluated at each stage. **(L)** Quantification of (i) *Dkk3-CE+* and *Prg4-CE+* cell number present in hyperplastic synovium (**L**, upper histograms) on day 7 after surgery and (ii) proliferative cell number in synovium (SL) and articular cartilage (AC) on day 7 before or after surgery (**L**, lower histograms) calculated as mean labeled cells/100 cells ± s.d., n=6, *P < 0.01. A, C, D, bar = 200 μm; B, bar = 4 mm; E–H, bar = 75 μm; and I–K, bar = 50 μm

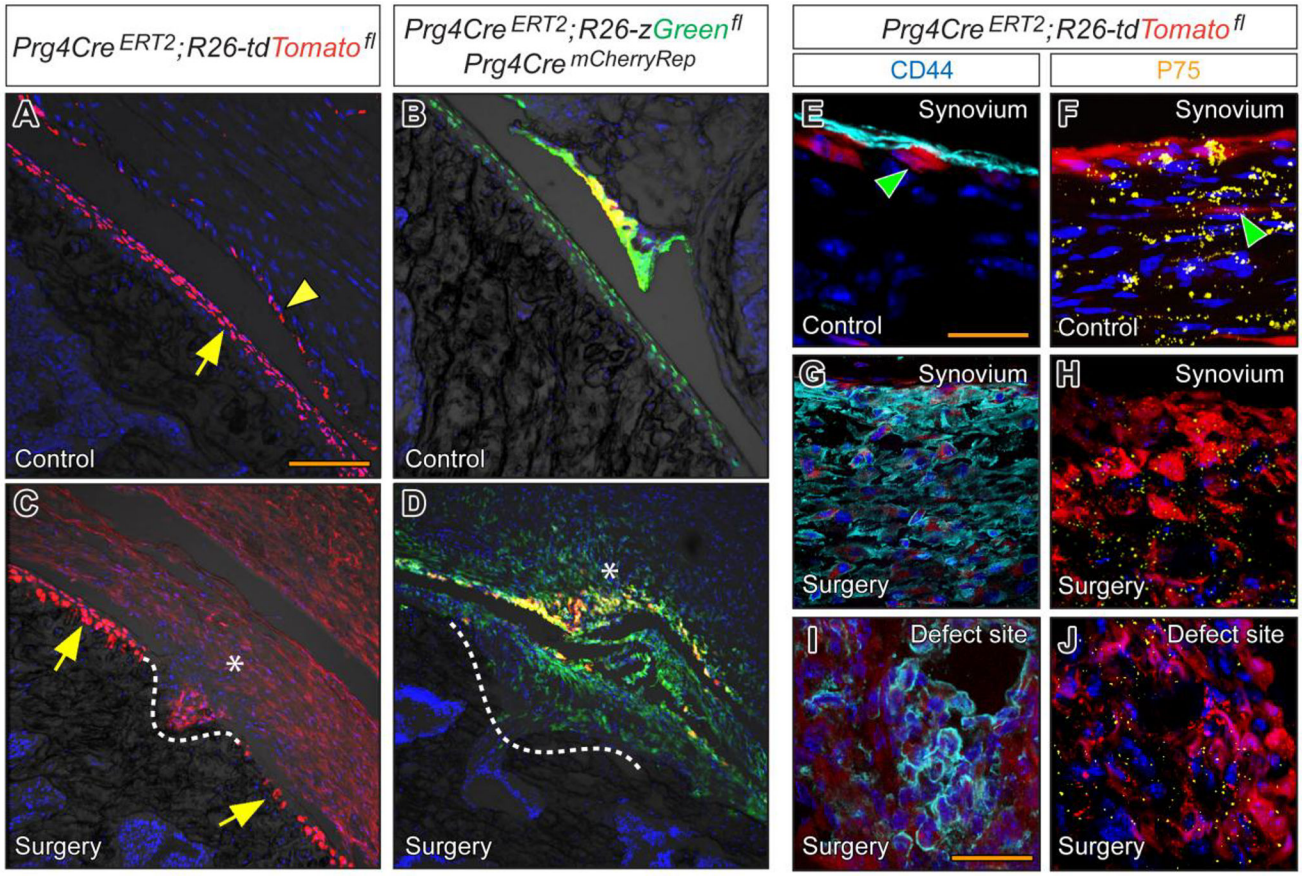

Fig. 6.

Prg4-CE+ progeny and real-time *Prg4*-expressing cells respond differently to acute joint injury. (**A–B)** After tamoxifen induction at P28, *Prg4-CE+*cells are restricted to synovial lining (arrowhead) and superficial layer of articular cartilage (arrow). **(B)** Real-time *Prg4mCherry* (red) expressing cells remain few in number and limited to articular and synovial surfaces. **(C–D)** *Prg4-CE+* cells become very numerous in the thickened synovium within 7 days from surgery (**C**, asterisk) and fill the injury defect (dashed line), but real-time *Prg4mCherry* (red) expressing cells remain few in number and limited to articular and synovial surfaces (**D**), with some exhibiting progeny plus real-time character (yellow). (**E–J**) In unoperated knees (**E–F**), synovial cells exhibit CD44 immunostaining (**E**, arrowhead), P75 immunostaning (**F**, arrowheads), and *Prg4-CE+* character. After 7 days from surgery, the number of positive cells greatly increases in synovium (**G–H**) and within defect site **(I–J)**. Images are representative of a minimum of 10 mice evaluated at each stage. A–D, bar = 75 μm; and E–J, bar =15 μm.

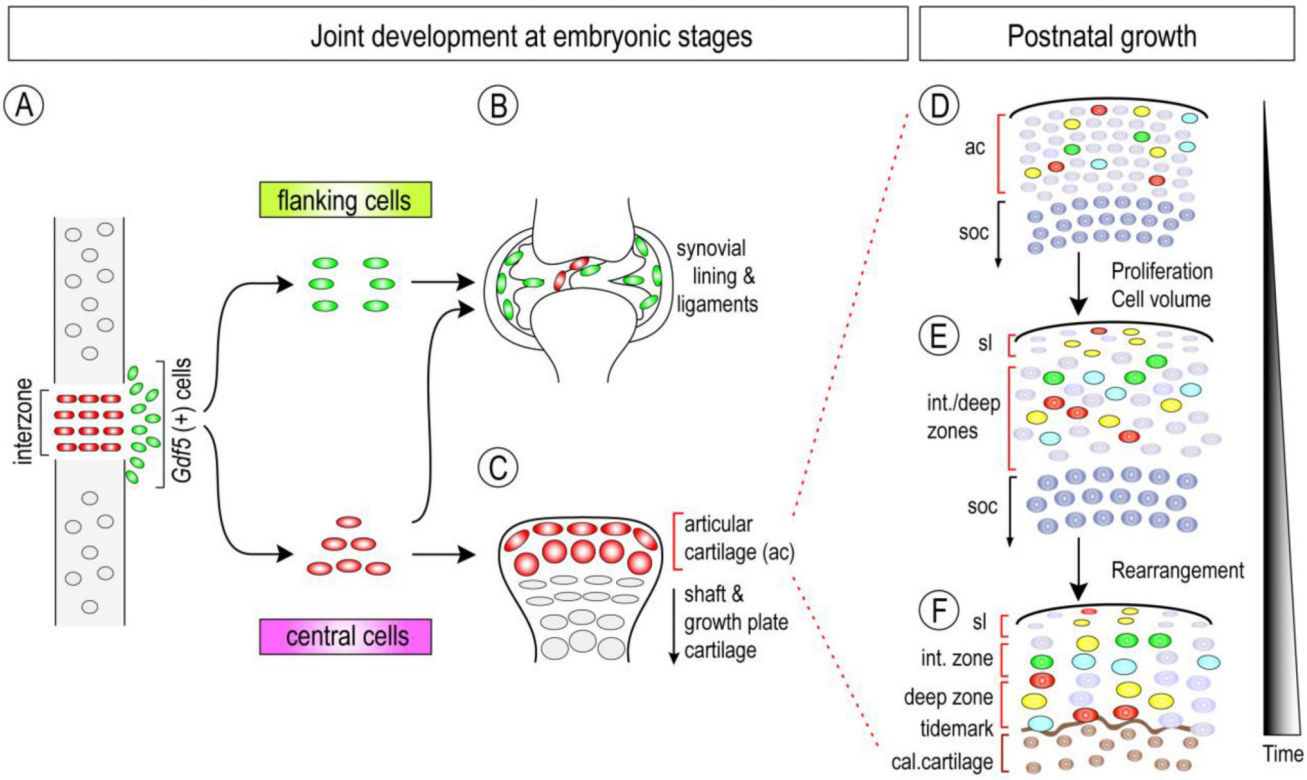

Fig. 7.

Model of synovial joint formation and postnatal growth and morphogenesis. **(A)** Mesenchymal *Gdf5+* cells constituting the interzone area at incipient joint sites in early embryonic limbs would comprise centrally-located descendants of chondrocytes (red color) and flanking cells recruited from surrounding tissues into the *Gdf5* lineage (green color). (**B–C**) Both populations would increase in number, but would not migrate significantly over time and would give rise to distinct local tissues, with the flanking cells largely producing synovial lining, capsule and peripheral ligaments and central cells generating articular cartilage and intrajoint ligaments. (**D–F**) Starting at neonatal stages and proceeding into adulthood, knee articular cartilage (ac) would progressively acquire its functional organization and structure that include: superficial layers (sl); intermediate (int.) and deep zones; and a tidemark overlaying the calcified (cal.) cartilage and secondary ossification center (soc). Growth in thickness would be driven by limited proliferation at neonatal stages (**D**) and by cell volume increases at subsequent stages (**E–F**). The characteristic cell stacks perpendicular to the articular surface would entail repositioning and intercalation of neighboring chondrocytes, producing stacks of non-daughter (and differently labeled) cells. We should note that as this schematic makes it clear, the model focuses on the central region of articular cartilage such as that occurring in the proximal tibia plateau. Additional and diverse mechanisms may be involved in development, thickening and expansion of articular cartilage in the lateral portions of the joints over postnatal life.